D-band Free Space Dielectric Characterization of a Low-Cost Ultradense Microdiamond Composite for Heat Spreading

Shu-Ming Chang[1], Chelsea Swank[2], Andrew Kummel[2], Muhannad S. Bakir[3], Mark Rodwell[1], James F. Buckwalter[1]

[1]University of California Santa Barbara, USA
[2]University of California San Diego, USA
[3]Georgia Institute of Technology, USA

Abstract—**Low-cost dielectric materials are needed above 100 GHz with low permittivity and loss tangent as well as significant thermal conductivity ($\sim$100 $W/m \cdot K$). A free-space measurement setup is demonstrated to characterize a proposed ultradense diamond composite material at D-band. We leverage free-space calibration with the NIST iterative method to extract the permittivity and loss tangent and compare this approach with other methods. Time-domain gating is employed to reduce the uncertainty in the free space characterization. Our measurement indicates the diamond composite offers a relative permittivity of 3.5 and loss tangent of 3×10^{-2} from 110-140 GHz. To the author's knowledge, this is the first report of diamond composite compatible with packaging requirements at D-band.**

Index Terms—**D-band, diamond composite, Free-space dielectric characterization, time-domain gating**

I. INTRODUCTION

D-band (110-170 GHz) offers opportunities for millimeter-wave radar and backhaul communications [1]. However, the spacing between antennas in beamforming systems is on the order of 1 mm, imposing significant space constraints. In Fig.1, a low-cost package might mount a silicon beamformer to one side of a printed circuit board while transitions through the board couple into a power amplifier (PA) array based on III-V MMICs capable of output power exceeding 100 mW. This scheme places two constraints on the package. First, the top side of the package must simultaneously offer excellent thermal dissipation as each PA dissipates one-half Watt. Second, the PAs on the top side must couple directly into antennas on the top side. Consequently, the D-band package requires a low-cost material that offers both excellent dielectric properties as well as high thermal conduction while allowing low-temperature processing.

Recently, D-band packaging has focused on glass and other insulating interposers such as silicon and aluminum nitride [2] [3]. Glass is not intrinsically a thermal conductor but copper thermal vias are employed since the thermal conductivity of bulk Cu is >400 W/m-K under ideal conditions. However, the thermal vias substantially increase the cost of the interposer. Other materials typically offer some compromise between thermal conductivity, loss tangent, and amenability with multi-layer packaging. An ideal thermal conductor would behave like bulk diamond (2000 W/m-K), but could be processed at low temperature and formed around PA chips.

Alternatively, an ultradense diamond composite (UDC) is formed from thermally-fused microdiamonds. The UDC com-
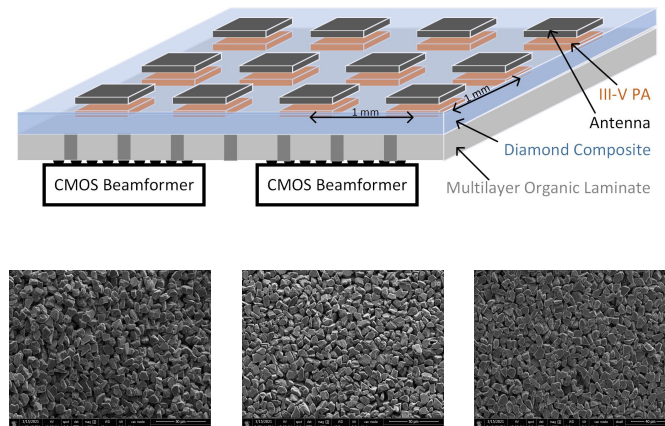

Fig. 1: Ultradense diamond composite deposited at low-temperature on a low-cost printed circuit board to remove heat from PA arrays. A 1000X SEM image shows the packing over time with applied ultrasound and heat during the formation of the diamond composites. (a) Composite is produced without ultrasonication and heat (b) 8 min of applied ultrasound and heat(60 C) (c) 16 min of applied ultrasound and heat.

prises 10-um synthetic diamond particles and trimethylpropane triacrylate (TMP-TA). The relative permittivity (ϵ_r) and loss tangent (δ) of bulk diamond and TMP-TA are 5.7 and 1.78 and 5×10^{-4} and 0.04, respectively [4]. To increase the packing density of the diamond, pressure is applied to a diamond slurry deposited into a 20-mm Al mold inside an ultrasonicator and processed at 60 C until the diamond composite formed. Once the diamond matrix of the diamond composite was complete, the composite was placed in an oven at 120C for 1 hr. Next, TMPTA was deposited into the diamond film and cured at a maximum 140C for 20 min. Fig. 1 shows SEM images of the UDC.

This paper investigates the dielectric properties of the UDC to understand whether the excellent properties of the original diamond are retained above 100 GHz for millimeter-wave packaging of arrays. In this work, we measure the UDC at D-band using a focused beam free-space measurement to characterize the dielectric properties [5]. Section II discusses the dielectric characterization method at D-band and Section III reports the UDC materials couples high thermal conductivity with low dielectric losses.
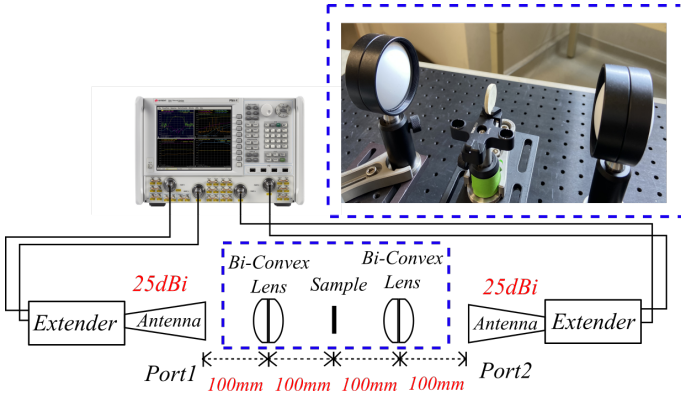
Fig. 2: Free Space Measurement Setup

Fig. 3: Free Space TRL calibration procedure

II. Free-space Dielectric Characterization

At D-band, the advantage of free-space characterization compared with a transmission line method is eliminating the uncertainty associated with the conductor losses and surface roughness. The D-band dielectric characterization system comprises a Keysight PNA with D-band frequency extenders, D-band horn antennas, bi-convex lenses, and positioning fixtures that allows free-space TRL calibration as illustrated in Fig. 2.

A. Biconvex Lens for D-band

Free-space characterization typically demands a relatively large sample area relative to the wavelength to minimize the system uncertainty due to the diffraction effect. If the sample size is small, a high-gain horn antenna produces a narrow beamwidth and the lens positions relative to the antenna and sample are critical. A bi-convex lens is constructed from two plano-convex lenses held together by a metal ring. Compared to a plano-convex lens, the combination of the bi-convex lens system reduces the focal distance by one-half and has the advantage to bring the antenna close to the lens while positioning focal distance at the sample. The distance between antenna and lens and the distance between lens and sample are twice the effective focal distance. By inserting a big metal plate close to the sample edge, the S-Parameters have not been interfered. It proves that the energy has been confined to the small diamond sample. Fig. 2 shows bi-convex lens and small diamond sample.

B. Calibration

Before calibration, alignment is performed by maximizing S_{21} signal. The free-space TRL calibration procedures follow recent work [6] [7]. Fig. 3 shows the calibration procedure. The through standard is achieved by keeping the distance between each element equal to twice of the focal distance and the reflect standard is achieved by placing a metal plate at the focal plane of the transmit and receive antenna, respectively. Due to the thickness of the metal, the second port lens and antenna are moved according to the metal thickness D. Finally, a line standard is achieved by separating the focal plane of the two antennas by a distance equal to a quarter wavelength of the free-space at the center frequency of the band.
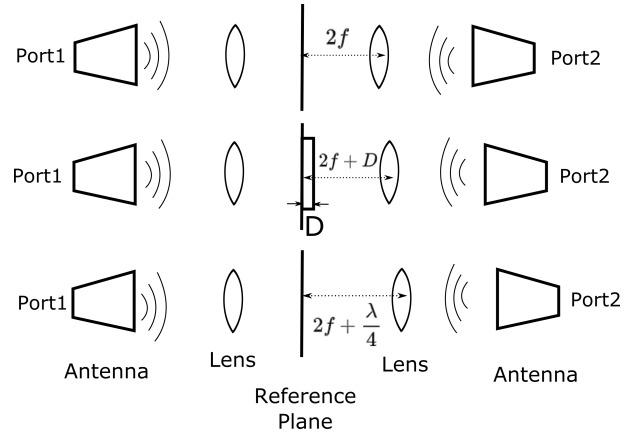
C. Extraction Method

In the focused-beam system, the energy is confined to an area within the sample to measure S-parameters. There are multiple extraction methods to characterize the dielectric using measured S parameters for the sample material. The NRW algorithm determines permittivity from S_{11} and S_{21} [8]. More recently, the NIST iterative algorithm was proposed using similar measurement data [9] [10]. The NIST iterative algorithm does not require precise placement of the sample relative to the calibration reference plane which is useful for D-band measurements, where a small distance movement can cause significant phase errors. The NIST iterative method utilizes all four S-parameters to determine permittivity from the matrix determinant.

$$S_{11}S_{22} - S_{21}S_{12} = \frac{\Gamma^2 - T^2}{1 - \Gamma^2 T^2}, \tag{1}$$

where Γ is the reflection coefficient at the surface of the sample and T is the transmission coefficient through the sample. The phase error due to sample placement will be eliminated, resulting in better accuracy compared to NRW algorithm. The reflection and transmission can be related to dielectric properties.

$$\Gamma = \frac{\gamma_0 - \gamma}{\gamma_0 + \gamma} \tag{2}$$

$$T = e^{-\gamma d} \tag{3}$$

where γ and d represent the propagation constant and thickness of the sample. Fig. 4 compares the NRW and NIST iterative method. As a baseline material with well-defined properties, a quartz wafer is adopted to verify the overall methodology. Five sets of quartz data are collected at different times with individual calibration data. While the NRW method produced inconsistent results due to positioning uncertainty during calibration process and different metal thickness as a reflection calibration standards, the NIST iterative method shows consistent characteristics over the the different samples and relative placement uncertainty. The NIST method is immune to phase errors and provides more consistent results,
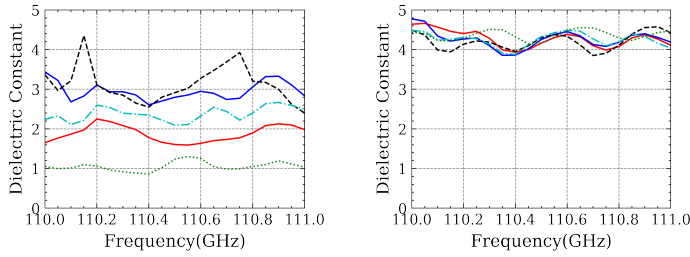
Fig. 4: Quartz wafer dielectric characterization extracted by (left) NRW method and (right) NIST iterative method at 110 GHz

Fig. 6: Quartz S_{11} in Time Domain with and without time-gating

Fig. 7: Quartz sample loss tangent with and without time-gating

however, we encountered a ripple in the measurement that was no mitigated through averaging across the measurements.

D. Time Domain Gating

Despite the high gain lens, multipath scattering introduces uncertainty that produces the ripple illustrated in Fig. 4. Consequently, we introduced time-domain gating of the S-Parameters to filter out non-dominant components and improve the accuracy of the extracted permittivity results. By separating different transmission components such as the desired signal, signals from the multiple reflections and from discontinuity within the measurement channel. This filter is a window that is convolved with the data to preserve the first strongest desired signal in time-domain while suppressing other signals at other times and then transfer back to frequency domain.

Fig. 5 and Fig. 6 shows quartz S_{11} magnitude data as an example in frequency domain and in time domain while iterative method needs all four S-Parameters, the remaining S-Parameters also need to adopt time-gating. The gated loss tangent results are much more smooth than the raw data. As an example, Fig. 7 is the quartz wafer loss tangent measurement results. Notably, time gating eliminates the significant ripple in the loss tangent. The measurement over 110 to 140 GHz indicates that the loss tangent is less than 6×10^{-3} while the loss tangent for quartz is expected to be less than 1×10^{-3} based on low-frequency characterization. We use this observation to define the measurement floor for loss tangent at 6×10^{-3}.
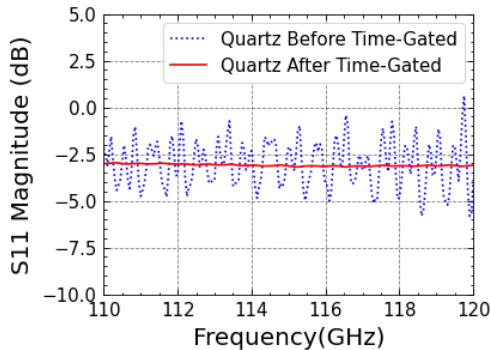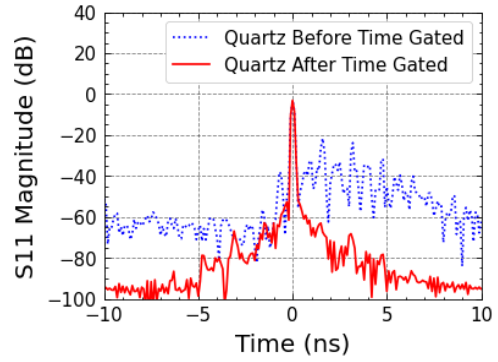

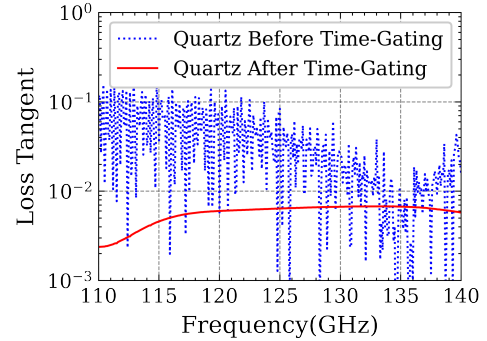Fig. 5: Quartz S_{11} in Frequency Domain with and without time-gating

III. MEASUREMENT RESULTS

The dielectric characterization of the UDC samples had thicknesses of 1.68 mm and 2.92 mm to confirm the intrinsic properties of the material. The diameter of the available samples is roughly 18 mm. Since the diamond sample thickness is not uniform, the measurement is repeated eight times to average the results. The NIST iterative method and time-domain gating are adopted to extract permittivity and loss tangent in Fig. 8 and Fig. 9. The relative permittivity of the UDC samples are ~ 3.5 and the measured loss tangents are $\sim 3 \times 10^{-2}$ in both 1.68mm and 2.92mm sample. The thicker sample has less uncertainty in dielectric constant and loss tangent before time-gating compared to the thinner sample while both the results after time-gating are similar. The results indicate that the permittivity is roughly 50% of diamond while the loss tangent is limited by the characteristic of the TMP-TA.

IV. CONCLUSION

A free-space material characterization is performed in D-band. We describe the material properties of an ultradense diamond composite as well as the free space TRL calibration, extraction methods, and time gating in the measurment. The NIST iterative methodology demonstrated consistency compared with other methods and time-domain gating eliminates measurement artifacts in the dielectric and loss tangent characterization. We conclude that the diamond composite can
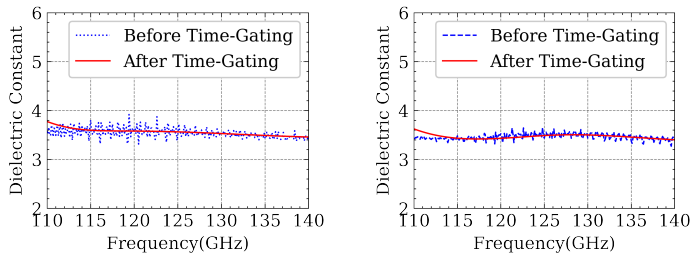
Fig. 8: Diamond composite sample dielectric constant with and without time-domain gating (left) 1.68 mm and (right) 2.92mm
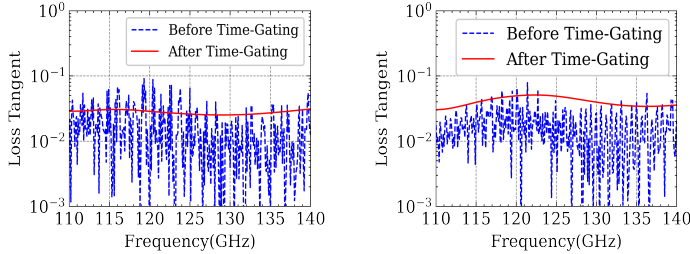

Fig. 9: Diamond composite sample loss tangent with and without time-domain gating (left) 1.68 mm and (right) 2.92mm

offer low dielectric permittivity and acceptable loss tangent while promising a thermal conductivity approximating bulk diamond.

REFERENCES

[1] M. J. W. Rodwell, "100-340GHz Spatially Multiplexed Communications: IC, Transceiver, and Link Design," 2019 IEEE 20th International Workshop on Signal Processing Advances in Wireless Communications (SPAWC), 2019, pp. 1-5, doi: 10.1109/SPAWC.2019.8815433.

[2] A. Singh et al., "A D-Band Radio-on-Glass Module for Spectrally-Efficient and Low-Cost Wireless Backhaul," 2020 IEEE Radio Frequency Integrated Circuits Symposium (RFIC), 2020, pp. 99-102, doi: 10.1109/RFIC49505.2020.9218437.

[3] M. Ito and T. Marumoto, "Silica-Based Packaging Structure for D-band RF module," 2018 IEEE/MTT-S International Microwave Symposium - IMS, 2018, pp. 871-874, doi: 10.1109/MWSYM.2018.8439218.

[4] Aziz, N.A.M., Yunus, R., Hamid, H.A. et al. An acceleration of microwave-assisted transesterification of palm oil-based methyl ester into trimethylolpropane ester. Sci Rep 10, 19652 (2020). https://doi.org/10.1038/s41598-020-76775-y

[5] D. K. Ghodgaonkar, V. V. Varadan and V. K. Varadan, "A free-space method for measurement of dielectric constants and loss tangents at microwave frequencies," in IEEE Transactions on Instrumentation and Measurement, vol. 38, no. 3, pp. 789-793, June 1989, doi: 10.1109/19.32194.

[6] N. Vohra and M. El-Shenawee, "K- and W-Band Free-Space Characterizations of Highly Conductive Radar Absorbing Materials," in IEEE Transactions on Instrumentation and Measurement, vol. 70, pp. 1-10, 2021, Art no. 8001910, doi: 10.1109/TIM.2020.3041821.

[7] N. Vohra, L. R. Rodriguez-Aguilar, J. S. Batista and M. El-Shenawee, "Free-Space Characterization of Radar Absorbing Non-Magnetic Materials in the W-Band," 2020 94th ARFTG Microwave Measurement Symposium (ARFTG), 2020, pp. 1-4, doi: 10.1109/ARFTG47584.2020.9071679.

[8] A. M. Nicolson and G. F. Ross, "Measurement of the Intrinsic Properties of Materials by Time-Domain Techniques," in IEEE Transactions on Instrumentation and Measurement, vol. 19, no. 4, pp. 377-382, Nov. 1970, doi: 10.1109/TIM.1970.4313932.

[9] J. Baker-Jarvis, E. J. Vanzura and W. A. Kissick, "Improved technique for determining complex permittivity with the transmission/reflection method," in IEEE Transactions on Microwave Theory and Techniques, vol. 38, no. 8, pp. 1096-1103, Aug. 1990, doi: 10.1109/22.57336.

[10] J. Baker-Jarvis, M. D. Janezic, J. H. Grosvenor, Jr., and R. G. Geyer, "Transmission/reflection and short-circuit line methods for measuring permittivity and permeability," NIST, Boulder, CO, USA, Tech. Note 1355-R, 1993.